NRC Research Press

ARTICLE

Reconstructing the deformation of the North Anatolian Fault Zone through restoring the Oligo–Miocene exhumation pattern of the Almacık Block (northwestern Turkey) based on the apatite (U–Th)/He ages[1]

Gürsel Sunal, Mehmet Korhan Erturaç, Pınar Gutsuz, István Dunkl, and Ziyadin Cakir

Abstract: The Almacık Block is an approximately 73 km long and 21 km wide tectonic sliver formed by the North Anatolian Fault Zone in northwestern Turkey. Morphologically, it is one of the most pronounced structures along the North Anatolian Fault Zone. All the segments bounding the Almacık Block were ruptured during the second half of the 20th century. The fifty-four apatite (U–Th)/He ages we obtained showed that the region including the Almacık Block was exhumed during the Oligo–Miocene interval and then original exhumation pattern was distorted by the North Anatolian Fault Zone during the Miocene to recent. To interpret this distortion and to reconstruct it to the original state, we modelled "Λ"-shaped mountain fronts in the most probable deformation scenarios. The block has been tilted southward about an approximately east–west-trending horizontal (slightly dipping to the east) axis. As a result of this rotation, the northern part of the block has been uplifted about 2800 m, whereas the southern part has subsided about 430 m, likely during the last 2.5 Myr. The exhumation in the studied region started at around 34 Ma and lasted until 16 Ma with a mean exhumation rate of about 60 m/Myr.

Key words: NW Turkey, Almacık Block, North Anatolian Fault Zone, apatite (U–Th)/He (data or age), rotation.

Résumé : Le bloc d'Almacık est un copeau tectonique de ~73 km de longueur et ~21 km de largeur formé par la zone de faille nord-anatolienne dans le nord-ouest de la Turquie. Du point de vue morphologique, il s'agit d'une des structures les plus prononcées le long de la zone de faille nord-anatolienne. Tous les segments qui limitent le bloc d'Almacık ont été le lieu de ruptures durant la deuxième moitié du 20e siècle. Cinquante-quatre âges (U–Th)/He sur apatite que nous avons obtenus montrent que la région qui comprend le bloc d'Almacık a été exhumée durant l'intervalle Oligocène–Miocène, puis que le motif d'exhumation initial a été distordu par la zone de faille nord-anatolienne du Miocène jusqu'à la période récente. Pour interpréter cette distorsion et reconstituer l'état initial du bloc, nous avons modélisé un front de montagnes en forme de « Λ » dans les scénarios de déformation les plus probables. Le bloc a été déversé vers le sud autour d'un axe à peu près horizontal (plongeant légèrement vers l'est) d'orientation E–O. Du fait de cette rotation, la partie nord du bloc a été soulevée sur ~2 800 m, alors que sa partie sud s'est affaissée de ~430 m, probablement durant les dernières 2,5 millions d'années. L'exhumation dans la région étudiée a débuté autour de 34 Ma et s'est poursuivie jusqu'à 16 Ma, à un taux d'exhumation moyen de ~60 m/million d'années. [Traduit par la Rédaction]

Mots-clés : nord–ouest de la Turquie, bloc d'Almacık, ZFNA, (U–Th)/He sur apatite (donnés ou âge), rotation.

Introduction

Apatite (U–Th)/He (AHe) and fission track (AFT) dating are frequently used methods in low-temperature thermochronological studies (e.g., Zattin et al. 2010; Stübner et al. 2018; Cavazza et al. 2018; Ballato et al. 2018). The low closure temperature of the AHe thermochronometer (around 60 °C, Farley 2002; Ehlers and Farley 2003) and the presence of apatite as an accessory mineral in many rock types have resulted in the use of this method in many tectonic studies. Considering a typical geothermal gradient (about 25 °C/km), this closure temperature corresponds to a depth of approximately 2–2.5 km (Farley 2002; Green and Duddy 2006). Therefore, it provides valuable age constraints for exhumation events and for the determination of exhumation rates. In this study, we aim to introduce the use of AHe ages to restore post-exhumation deformations such as post-collisional strike-slip faults.

The North Anatolian Shear Zone (NASZ) extends about 1600 km between the Karlıova Triple Junction in the east and the northern Aegean in the west, roughly parallel to the Black Sea coast (Barka, 1992; Ketin, 1948 and 1969; Şengör, 1979; Şengör et al. 2005; Şengör and Zabcı 2019) (Fig. 1). This dextral shear zone is confined to the Tethyside accretionary complexe that generally widens from east to west in northern Turkey, reaching its maximum

Received 9 November 2018. Accepted 17 May 2019.

Paper handled by Ali Polat.

G. Sunal, P. Gutsuz, and Z. Cakir. Istanbul Teknik Üniversitesi, Jeoloji Mühendisliği Bölümü, 34469 Istanbul, Türkiye.
M.K. Erturaç. Sakarya Üniversitesi, Fen Edebiyat Fakültesi, Coğrafya Bölümü, 54187 Sakarya, Türkiye; Sakarya Universitesi Araştırma, Geliştirme ve Uygulama Merkezi (SARGEM), Esentepe Kampüsü, 54187 Sakarya, Türkiye.
I. Dunkl. Sedimentology and Environmental Geology, Geoscience Center, University of Göttingen, Goldschmidtstrasse 3, D-37077 Göttingen, Germany.
Corresponding author: Gürsel Sunal (email: gsunal@itu.edu.tr).

[1]This paper is part of a Special Issue entitled "Understanding tectonic processes and their consequences: a tribute to A.M. Celâl Şengör".

Fig. 1. (*a*) Simplified tectonic map of the Almacık Block and its surroundings (modified after Bozkurt et al. 2013). The block is fusiform and bounded entirely by the branches of the North Anatolian Fault Zone (NAFZ). (*b*) Detailed structural and post-Paleocene outcrop map of the Almacık Block (after Gedik and Aksay 2002). Note that Eocene units commonly cover tectonic units in the İstanbul and Sakarya Zones and there is no Miocene unit in the Almacık block, as during that interval the block exhumed. Active faults are from Emre et al. (2011). AM, Almacık metamorphics; IPSZ, Intra-Pontide Suture Zone. [Color online.]

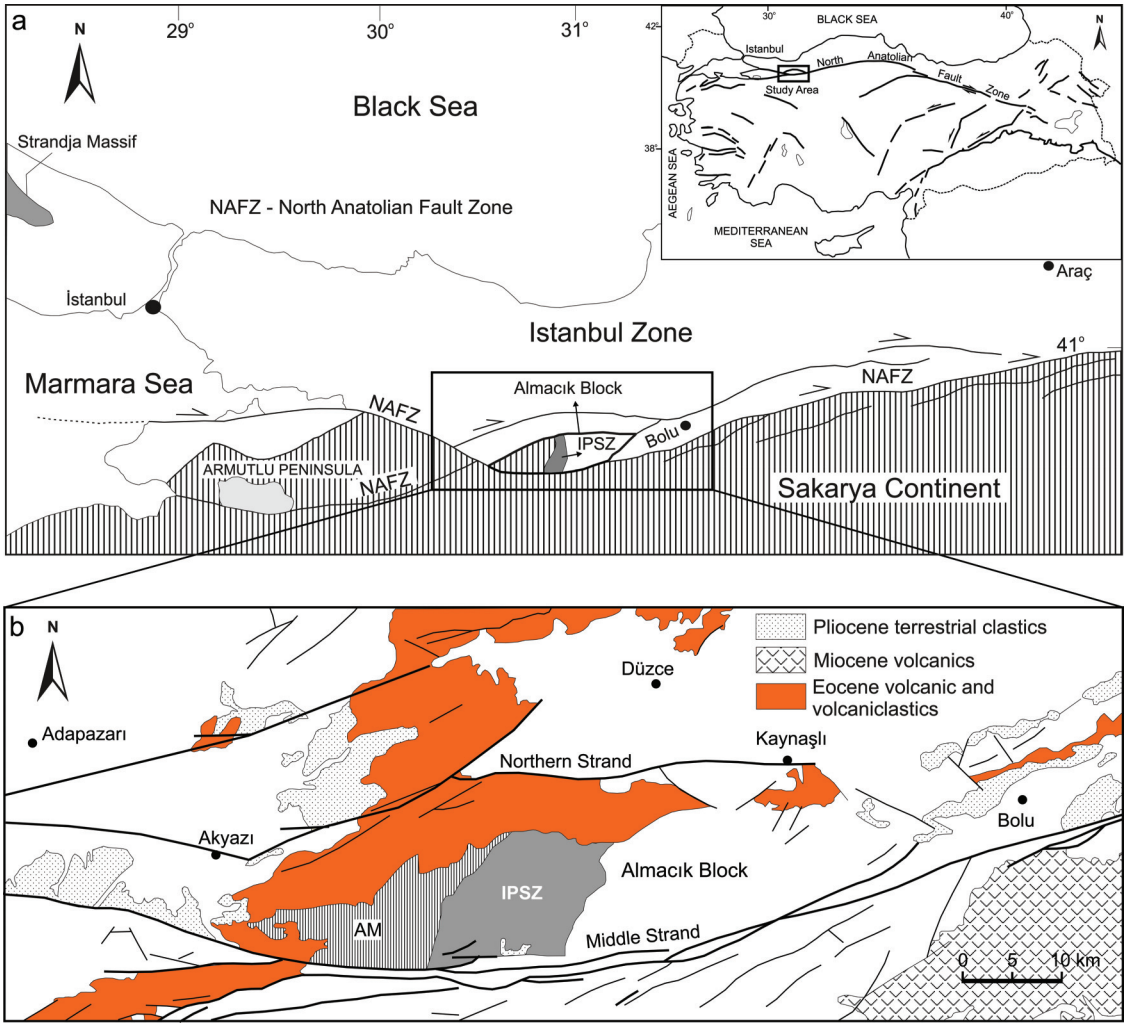

width of about 100 km in the Marmara Region (Şengör et al. 2005; Şengör and Zabcı, 2019). The widening of the deformation zone is also well defined by the multi-strand structure of the North Anatolian Fault (NAF) (Barka and Kadinsky-Cade, 1988; Şengör et al. 2005). The Almacık Block is a well-documented fault-bounded block in the NAF system (Barka 1992; Şengör et al. 2005) (Fig. 1). For the purposes outlined above, we focus on the Almacık Block bounded by the active northern and the middle strands of the North Anatolian Fault Zone (NAFZ) that was ruptured with five large earthquakes (Ms >7.0) during the last century (1944 Gerede, 1957 Abant, 1967 Mudurnu Valley, 1999 İzmit and Düzce earthquakes; see Ambraseys and Zatopek 1969; Barka 1992, 1996; Kondo et al. 2005, 2010; Duman et al. 2005; Pucci et al. 2007; Akyüz et al. 2002; Çakır et al. 2003*a*). Another important feature of the Almacık Block is that it represents an elevated mountain peak (about 1650 m) in an east–west-trending mountain range, namely the Bolu-Ilgaz Mountains that are about 300 km long and up to about 2000 m high. This mountain range preserves the pre-NAFZ history of the whole northern part of Anatolia. This range formed in the Oligocene (see Sunal and Erturaç 2012 for a review) after the closure of the northern branch of the Neotethys ocean and due to subsequent compression (Şengör and Yılmaz 1981, see also Keskin et al. 2008 for a review). In the Eocene, almost the entire Izmir–Ankara–Erzincan Suture Zone (IAESZ) was covered by marine turbidites overlain by volcanic and volcaniclastic deposits. This succession is generally thicker than 2 km in most places, such as in Ganos Mountain, where apatite fission-track dating was applied on a >4 km thick sequence (Zattin et al. 2005 and 2010). All tectonic units exposed in and around the Almacık Block are covered by Eocene sequences (Fig. 1). The post-Eocene burial reset the AHe system in the basement and thus it is possible to determine the age of the onset of exhumation in this block, which was the main goal of our study. The second aim was to extract NAFZ-related deformation using the AHe cooling age pattern as a frame of reference. This is an indirect way to understand of the behavior of the NAFZ in this region. To elucidate the exhumation history, we performed apatite He thermochronology both from the northern part of the Middle Strand of the NAFZ (from the Almacık Block) and southern part of the Middle Strand of the NAFZ (from the Sakarya Zone). Although there have been attempts to restore later deformations using former exhumation data, especially in extensional regions (e.g., Fitzgerald and Gleadow 1990; Stockli, 2005 and references therein; Fitzgerald et al. 2006), studies dealing with large continental strike-slip faults post-dating collisional

orogenies are rare. Therefore, this study gives a new perspective on the evaluation of deformation phases that follow exhumation.

Geology of the region

The Almacık Mountain is a fault-bounded lensoidal block, where the block and the immediately adjacent region are characterized by different tectonic zones of northwestern Anatolia. To the north of the block (north of the northern branch of the NAFZ) (Fig. 1) is the Istanbul Zone, exposed with a Precambrian metamorphic basement (Chen et al. 2002) and unconformably overlying Ordovician arkoses and quartz arenites and Carboniferous chert and flysch (Lom et al. 2016). In contrast, the southern side of the block (south of the Middle Strand of the NAFZ) (Fig. 1) is composed of the rocks of the Sakarya Zone (Okay and Göncüoğlu 2004). The Sakarya Zone includes Jurassic volcanic and volcaniclastic rocks of the Mudurnu Formation (Altıner et al. 1991; Genç and Tüysüz 2010), Upper Jurassic–Lower Cretaceous limestones (Abdüsselamoğlu 1959) and Upper Cretaceous–lower Eocene wildflysch deposits with giant blocks of limestones and granitoids (for a detailed geological map of the region see supplementary Fig. S1[2]).

In the Almacık Block, both the Istanbul and the Sakarya zones are exposed and separated by a suture zone called the Intra-Pontide Suture Zone (IPSZ). The age of the suture is given as early Eocene (Cuisian (late Ypresin), Akbayram et al. 2016). In contrast with the southern part of the Almacık Block, there is a metamorphic succession in the western part of the block (Fig. 1) that is also assigned to the Sakarya Zone (Bozkurt et al. 2013). These schists, calc-schists, and marbles are Late Jurassic to Early Cretaceous in age (Çelik et al. 2009; Akbayram et al. 2013). The IPSZ is located in the center of the block with a roughly north–south alignment. The IPSZ contains metamorphosed ophiolitic rocks such as amphibolites, serpentinites, and meta-trondhjemite dykes (Bozkurt et al. 2013). Ordovician quartz arenites of the Istanbul Zone are exposed in the eastern part of the block, a large portion of which is covered by the Upper Cretaceous–lower Eocene wildflysch deposits (MTA map, Gedik and Aksay 2002) that contains marble, chert, and Precambrian granitoid blocks.

All units constituting both the Almacık Block and southern part of the Middle Strand of the NAFZ are transgressively overlain by a common cover of Eocene volcanic and volcaniclastic formations.

There are several published reports on the deformation of the Almacık Block (Şengör et al. 1985; Sarıbudak et al. 1990; İşseven et al. 2009 and Yıldırım and Tüysüz 2017) during the development of the NAFZ in the region. According to Şengör et al. (1985), considering the position of the IPSZ (Cuisian (Late Ypresin), Akbayram et al. 2016*b*), the Almacık Block underwent a 110° clockwise rotation around a vertical axis. Sarıbudak et al. (1990) proposed a much greater clockwise rotation of about 212° (from the paleomagnetic measurements from the Eocene volcanics). However, recent studies claim that the amount of the rotation is between about 20° (Yıldırım and Tüysüz 2017) and 28° (İşseven et al. 2009) clockwise. İşseven et al (2009) reported the rotation based on paleomagnetic measurements from Eocene volcanic rocks, whereas Yıldırım and Tüysüz (2017) used much younger morphological features (Pliocene–Pleistocene river incisions) to calculate the rotation. Hisarlı et al. (2011) proposed a counterclockwise tectonic rotation of 22.3° ± 7.8° (from paleomagnetic data from the middle Eocene volcanics) in the Almacık Block relative to the Istanbul Zone.

Sampling and analytical techniques

In the Almacık Block, the samples were collected from the metamorphic formations of the Sakarya Zone and from Upper Cretaceous flysch and Eocene volcanic and volcaniclastic formations developed in the İstanbul Zone (supplementary data Table S1[2]). Elevations of the samples range from 554 to 1568 m. All the samples collected from the southern part of the Middle Strand of the NAFZ are from rocks of the Sakarya Zone (Fig. 1). In the western part of the area, mainly Upper Cretaceous flysch and its blocks were sampled. Some additional samples were collected from Middle Jurassic volcanics and volcanogenic sandstones of the Mudurnu Formation with elevations ranging between 116 and 1471 m.

The quality of the dated samples was checked for possible secondary fluid effects. Samples were fresh and lacking apparent fluid alteration. The AHe analyses were performed at the GÖochron Laboratory at the University of Göttingen (Göttingen, Germany). Single-grain apatite aliquots were dated, usually three aliquots per sample. The crystals were selected carefully; only fissure-free grains were used, with well-defined completely convex external morphology. Shape parameters (such as length of prism, and total length and width of the crystals) of preferred euhedral crystals were determined and archived using multiple digital microphotographs. The crystals were wrapped in approximately 1 × 1 mm platinum capsules which were heated using an infrared laser. The extracted gas was purified using a SAES (Florence, Italy) Ti–Zr getter at 450 °C. The chemically inert noble gases and a minor amount of other rest gases were then expanded into a Hiden triple-filter quadrupol mass spectrometer (Hiden Analytical Inc., Livonia, MI, USA) equipped with a positive ion-counting detector. Beyond the detection of helium, the partial pressures of some rest gases were continuously monitored (H_2, CH_4, H_2O, N_2, Ar, and CO_2). Crystals were checked for degassing of He by sequential reheating and He measurement. Following degassing, samples were retrieved from the gas extraction line, spiked with calibrated ^{230}Th and ^{233}U solutions and dissolved in 2% HNO_3. Each sample batch was prepared with a series of procedural blanks and spiked normals to check the purity and calibration of the reagents and spikes. Spiked solutions were analyzed by a Perkin Elmer (Waltham, MA, USA) Elan DRC II inductively coupled plasma mass spectrometer (ICP-MS) with an APEX microflow nebulizer. Sm, Pt, and Ca were determined by external calibration. The ejection correction factors (F_t) were determined for the single crystals using a modified algorithm of Farley et al. (1996) with an in-house spreadsheet.

Results

Apatite (U–Th)/He dating

Twenty-four samples were dated from the Almacık Block and 30 samples from the southern part of the Middle Strand of the NAFZ (supplementary data Tables S1 and S2[2], respectively). Granitoids and metabasic rocks yielded the most and best apatite crystals, but apatites from the Upper Cretaceous flysch and the Middle Jurassic Mudurnu Formation (Altıner et al. 1991) also contained euhedral crystals suitable for dating, as they were fed by adjacent arc-derived rocks with short transport.

The unweighted sample mean ages revealed three groups: >36 Ma, 33–16 Ma, and 12–2.5 Ma (Fig. 2; supplementary data Table S2[2]). The oldest AHe age of the Almacık Block (~65 Ma, sample MK38 not shown in Fig. 2*a*) was obtained from the base of the Eocene sedimentary cover (see Figs. 1 and 3). The remaining older ages were from the southern part of the Middle Strand of the NAFZ (Figs. 2 and 3; supplementary data Table S2[2]), which is oriented roughly northeast to southwest. The second age group is the largest one and was obtained from different elevations (between 600–1600 m). Only two ages in the Almacık Block belong to the youngest group: samples MK57 and MK61 that gave ages of 10.7 ± 0.2 and 7.0 ± 1.3 Ma, respectively. The remaining younger ages are located in the southeastern part of the Middle Strand of the NAFZ

[2]Supplementary data are available with the article through the journal Web site at http://nrcresearchpress.com/doi/suppl/10.1139/cjes-2018-0283.

Fig. 2. Apatite (U–Th)/He age vs. elevation plots (*a*) data from the Almacık Block, and (*b*) south of the Middle Strand of the North Anatolian Fault Zone (NAFZ) (see the text for a detailed discussion). Numbers are the sample numbers given in Supplementary Table S2[2]. "f" indicates a fault (note that they have no geographical information just separation lines); the "?" next to some of the sample numbers indicates uncertain ages (see Supplementary Table S2[2]).

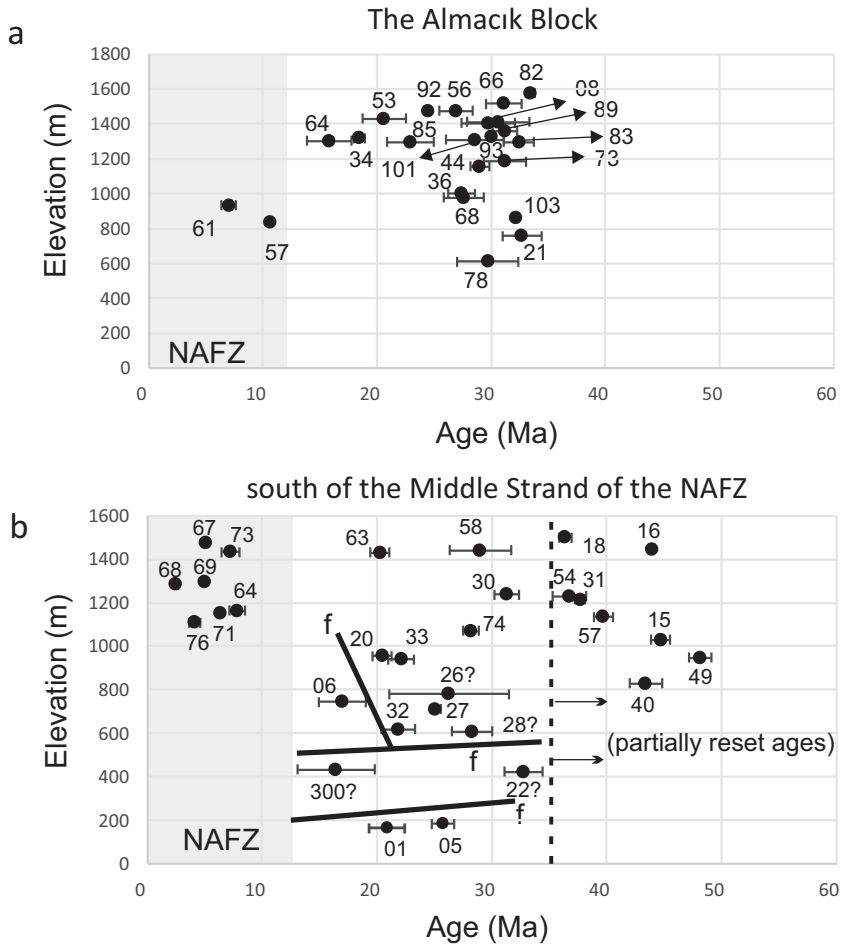

(Fig. 3). They cluster in a region where northeast–southwest-trending faults are present and range in elevation between 1100 and 1500 m (supplementary data Table S1[2]).

Discussion

Data interpretation and reduction

The age–elevation relationships (Fig. 2) do not show a well-developed simple and single correlation trend. The most critical constraint for the evaluation of the AHe data is the ca. 36 Ma thermal overprint event. Ages older than this threshold are interpreted as partially reset data. As described earlier, the Eocene deposits are the key units not only for the study region, but also for all the northern parts of Anatolia. After the closure of the IAESZ during the Paleocene, the entire region was covered by thick Eocene turbidites deposited in intramontane basins (49.3+2 to 38.1+1.9 Ma, Gülmez et al. 2013). Therefore, the ages older than 36 Ma (the lower radiometric age of the Eocene unit) represent the partially reset pre-burial ages. For this study, the same assumption was made; that is, that Eocene deposition caused reburial of the whole region and the reset of older He ages.

The studied region is controlled by the NAF that is thought to have initiated in the late Miocene (~12 Ma; Şengör et al. 2005), but the ages of displacements along its strike are not well known. Furthermore, Şengör et al. (2005) claim that before the NAF became a single narrow fault zone, it had already existed as an early, broader shear zone running roughly parallel to the IAESZ. This dextral shear zone (the NASZ) then evolved into the NAFZ that initiated in the east and then migrated to the west (Şengör et al. 2005). Therefore, the onset of the zone was almost synchronous all along the NAFZ (~12 Ma) but its activity as a single fault was diachronous. Consequently, the ages younger than 12 Ma are probably related to the NAFZ activity in the region. The possible meaning of the youngest age group is discussed in the section *Evolution of the Almacık Block in the NAFS*.

We observe two positively correlated age versus elevation trends in the Almacık Block and a rough one in the southern part of the Middle Strand of the NAFZ (Figs. 2*a* and 2*b*). In the Almacık Block, the one with a low exhumation rate is much more pronounced than the higher one.

The distribution of the AHe ages in age–elevation graph belonging to the southern part of the Middle Strand of the NAFZ is much more complicated (Fig. 2*b*). The age data in the southern part of the Middle Strand of the NAFZ have a wide scatter and the area is dissected by several branches of the NAFZ (Fig. 3). The separation lines that represent the faults observed in the field are roughly drawn in the graph in Fig. 2*b*. Note that they contain no geographical information, just separation lines distinguishing the ages that are the same as the faults observed in the field.

The range of ages is considerably wider than can be expected from the uncertainties of the analyses. There are two exhumation trends in the Almacık Block that cannot be explained spatially because they are next to each other. Furthermore, the distribu-

Fig. 3. Apatite (U–Th)/He ages (Ma) plotted on the digital elevation model of the study area (DEM data from NASA JPL 2013). Black dots represent samples from the Almacık Block, whereas white dots are from the south of the Middle Strand of the North Anatolian Fault Zone. White numbers with black backgrounds indicate less reliable age data (see the text for a detailed explanation).

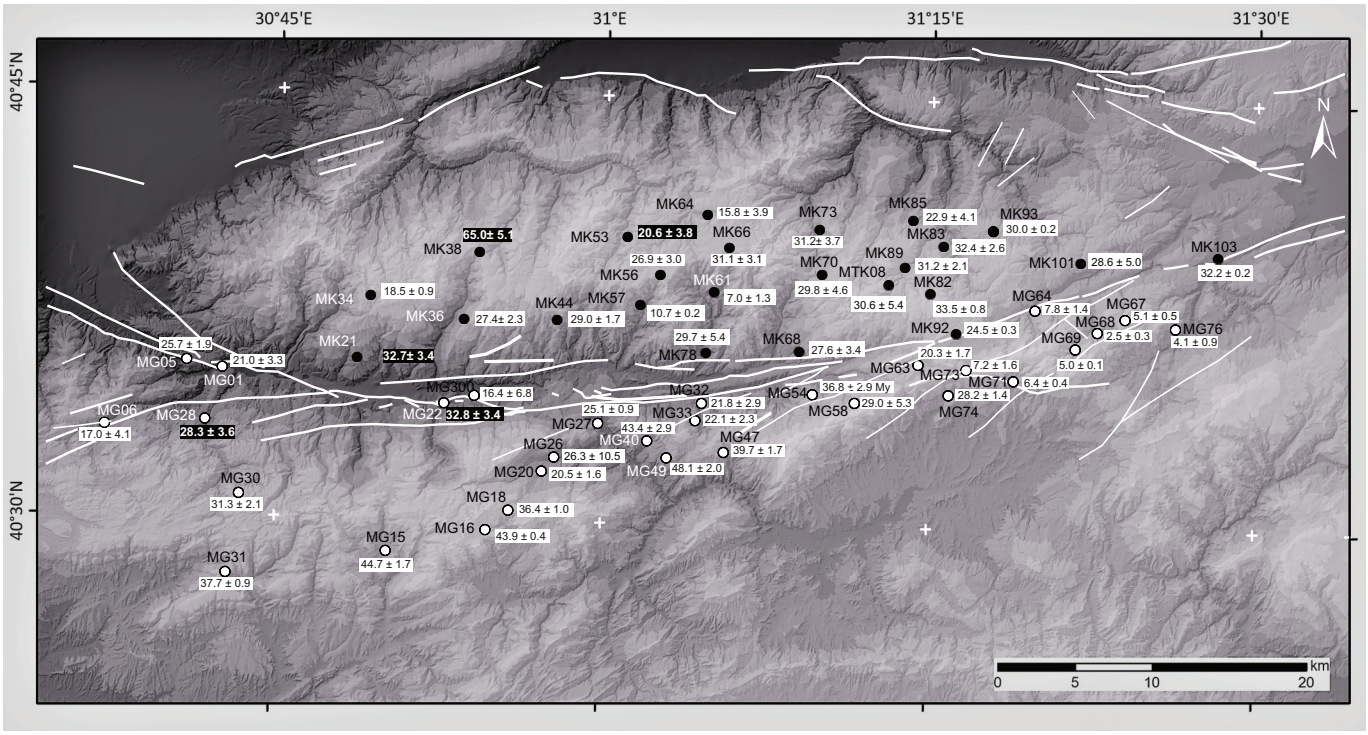

tion of the data in the southern part of the Middle Strand of the NAFZ has a zonal distribution similar to the higher exhumation rate in the Almacık Block. We hypothesize that the region studied here was exhumed at a steady rate until the onset of displacement along the NAFZ. To test this idea, we created a synthetic dataset with a specific exhumation rate and distorted it using common geological deformational structures.

Post-deformational styles of the exhumation data

For the sake of simplicity, we applied a constant exhumation rate, as in the case of curvilinear trends solutions can be much too complicated. Because the ages are constant and the only variable is the elevation, the dip of the deformed block (the surface that includes isochrones) is a direct indication of the change in the exhumation rate. There is a linear relationship between the dip of the surface of the mountain front and the exhumation rate.

We first illustrate the terminology used in the following figures and explanatory texts. Figure 4 shows elements of a synthetic exhumation dataset and relevant terms. On the right side of Fig. 4 we designed a mountain range profile (the north–south topographic section is real and taken from in the middle section of the Almacık Block) and for more simplicity, it is also schematized as a "Λ" shape. Every ascending sample from parts of the earth at depths deeper than the partial retention zone (PRZ), has a travel time indicating an age that marks its pass from the apatite closure temperature (~60 °C isotherm). The intersection between elevation (morphology) and different 60 °C isotherms creates isochrones of different ages (left side of Fig. 4). Those isotherms or isochrones do not represent a flat surface, rather they have upward concave shapes under the mountains (Farley 2002; Ehlers and Farley 2003; Reiners et al. 2003, 2017). Note that the amplitude of the isotherms is not the same as the amplitude of the mountain profile ("Λ") because the recent morphology of the Almacık Block formed after the NAFZ dissection, but the shape of the isotherms formed when the Almacık Block was a part of a larger mountain range. Therefore, today's morphology of the Almacık Block has a high amplitude and low wavelength (approximately 1.5 km and 20 km, respectively), but when its position was deeper, below a large mountain range during the Oligo–Miocene, isotherms formed relatively lower amplitudes and longer wavelengths (>1.5 km and >80 km, respectively, see Akbayram et al. 2016*a*, their fig. 3*c* for post-Eocene restoration of the region). However, we do not know the real shape (amplitude and wavelength) of the isotherms.

Assuming rotation

The first deformation style we consider here for the distortion of original exhumation data is rotation. There are three possible geometries: rotation about the vertical axis, rotation about the horizontal axis, and a combination of the two (oblique axis). The rotation about the vertical axis does not alter the relative position of samples unless it combines with other deformation styles. In contrast, the rotation about the horizontal or oblique axes including tilting and some sort of folding significantly changes the exhumation pattern. In Fig. 5, we applied rotation to a "Λ"-shaped theoretical mountain profile (we call it as a pyramid) about the horizontal axis. All the scenarios in this figure represent different types of rotation about the horizontal axes. In the cases shown in Figs. 5*a* and 5*b*, the rotation axes are set parallel to the t2 isochrone on the right side, but with a different sense of movements, one being clockwise and the other counterclockwise. Because the rotation axis is on one side (right flank (F1)) of the pyramid, the apparent exhumation rates increase rotating around the t2 isochrone (rotation axis) in the clockwise sense when compared with the original exhumation rate of the flanks. However, the apparent exhumation rate of both flanks decreases in a counterclockwise rotation state. When we again put the rotation axes parallel to the t1 isochrone instead of t2 (parallel to the lower corner), we have similar results with the previous situations, except for rotation of the data in the graphs that occur along different rotation axes (Figs. 5*c* and 5*d*). If there is no information about the initial stage of the data, there is no way to distinguish them. Similar results are

Fig. 4. Theoretical background and the terms used in the text. The illustrated north–south topographic profile is from the middle part of the Almacık Block. PRZ, partial retention zone. [Color online.]

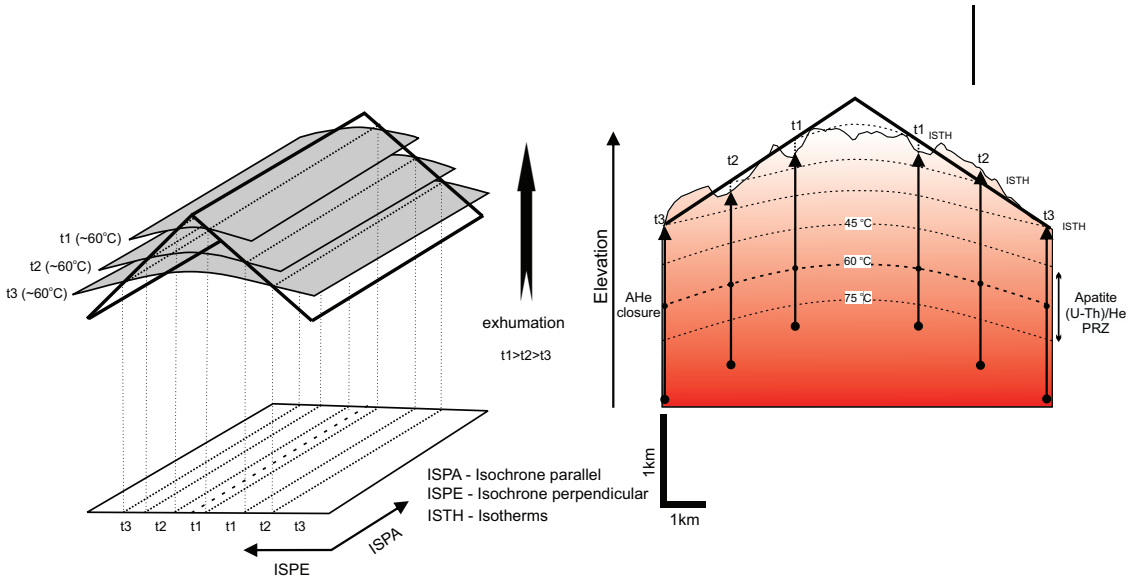

obtained when the rotation axes are placed parallel to the crest, along with the t1 isochrone (Figs. 5*e* and 5*f*). Note that here the original state of the trend line in the graph stays inside of those that are distorted, whereas in the previous states they either crosscut one of the later trends or align outside of them. The common features of the patterns of those distorted trends are a wedge-shaped appearance and a pinching out t3 isochrone.

In the final step of the rotation, rotation axes are designed as perpendicular to the isochrones (Figs. 5*e* and 5*f*). In both clockwise and counterclockwise situations, they reveal zonal distribution (ages are dispersed in a zone) rather than a wedge-like shape.

In the evolution of the Almacık Block, rotation about a vertical axis was proposed by several paleomagnetic studies (Şengör et al. 1985; Sarıbudak et al. 1990; İşseven et al. 2009; Yıldırım and Tüysüz 2017). Thus, we applied vertical and horizontal stepwise rotations on a north-dipping side of the pyramid (Fig. 6). For the sake of simplicity, we show only one side of the pyramid, as the other side will be the opposite. In each step, there is a 5° counterclockwise rotation about the vertical axis and 1° southward tilting (rotation around the horizontal axis) with the vertical axis being located in the center of the block. Furthermore, the horizontal axis is designed in the middle of the block, parallel to the longer sides of the block (Fig. 6). In this situation, increasing rotation and tilting lead to widening of the data (zonal distribution), lowering of the apparent exhumation rate, and finally the reversal of the age versus elevation correlation (negative correlation). The sense of rotation about the vertical axis does not affect the evolving distortion, but if we change the tilt direction from south to north, the rate of the exhumation increases and finally becomes vertical (not shown here). The reversal pattern of the exhumation rate depends on the style of deformation. For example, tilting via any kind of faulting does not create any reversal in the exhumation trend, but the formation of an overturned limb of a mega-scale fold can.

Assuming faulting

Compared with the rotational scenarios, the simulation of faulting results simpler patterns (Figs. 7*a*–7*d*), except for some combination of both rotation and faulting (Figs. 7*e* and 7*f*). A clear offset is observed in the case of dip-slip faults (normal or reverse) when their strikes are placed parallel to the long side one of the flanks (along with the isochrones) (Figs. 7*a* and 7*b*). Instead of an offset, a repetition occurs when faults' strikes are positioned perpendicular to the long side of one of the flanks (perpendicular to the isochrones) (Figs. 7*c* and 7*d*). However, it should be noted that because the fault crosscuts only one of the flanks, the offset occurs only along one flank that is not altered. In isochrone parallel situations, a rotation occurs synchronously in the footwalls of the faults if we have listric (e.g., detachment faults, Fig. 7*e*) or imbricated (thrust faults, Fig. 7*f*) faults. Additionally, it should be kept in mind that in domino-type normal faults and in duplicated thrust faults, accompanying rotation with an offset should be expected.

Zonal data distribution (repetition of the data to create a zone) was observed in all isochrone perpendicular situations (Figs. 5*e* and 5*f*, 6*b*–6*g*, and 7), but distortion in the fault situations had only twinning (or duplication) rather than zonal dispersion (Figs. 7*e* and 7*f*). In pure strike-slip faults (Figs. 7*g* and 7*h*), any changes can occur because there is no vertical movement during the fault activity. However, oblique faults can generate very complicated patterns.

The Almacık Block case

In the previous sections, some possible (common) deformation styles affecting the former exhumation trends are outlined. Here, we would like to interpret our thermochronological data from the Almacık Block in the light of the deformational scenarios discussed above.

In this study, we planned to collect data not only from the Almacık Block but also south of it (south of the Middle Strand of the NAFZ). The main reason is that rotational deformations of the Almacık Block are known from the literature but the area south of the Middle Strand of the NAFZ, where there is no information about a rotation or vertical movement, has only strike-slip faults (Fig. 3). Our expectation was to get a less distorted and simple exhumation trend in this area, but it turned out that it was complicated as well (Figs. 2 and 8), expressing a post exhumation deformation history. Therefore, during the data reduction, ages related to the NAFZ, PRZ, and those isolated in different fault-bounded domains were discarded. The distribution of the remaining ages shows a zonal pattern in the southern domain. As previously illustrated, the zonal distribution generally occurs in the isochrones with perpendicular rotation (Figs. 5*e* and 5*f* and 6*c*–6*g*) and isochrones with perpendicular offset of dip-slip faults

Fig. 5. Different rotation scenarios along the horizontal axes, which affect the exhumation pattern significantly. (*a*–*f*) Isochrone parallel (ISPA) axes, and (*g* and *h*) isochrone perpendicular (ISPE) axes. Original data are shown as white solid circles, whereas distorted data are illustrated as black solid circles. See the text for a detailed discussion. "F" indicates the flanks of the "Λ", and "t" indicates time. CW, clockwise; CCW, counterclockwise; RP, rotation pole; ZD, zonal distribution.

Fig. 6. Plan view of inclined relief with artificial points of different elevations and corresponding AHe ages. For simplicity, we calculated only one flank of the "Λ"-shaped mountain profile. 5° counterclockwise rotation around the vertical axis and 2° clockwise rotation along the horizontal axis were applied in every step. The sense of the rotation along the vertical axis does not change the results but rotation along the horizontal axis does. If counterclockwise rotation along the horizontal axis is be applied, the rate of the exhumation increases. The combination of both rotations creates zonal distribution and increases the change in the rates of exhumation.

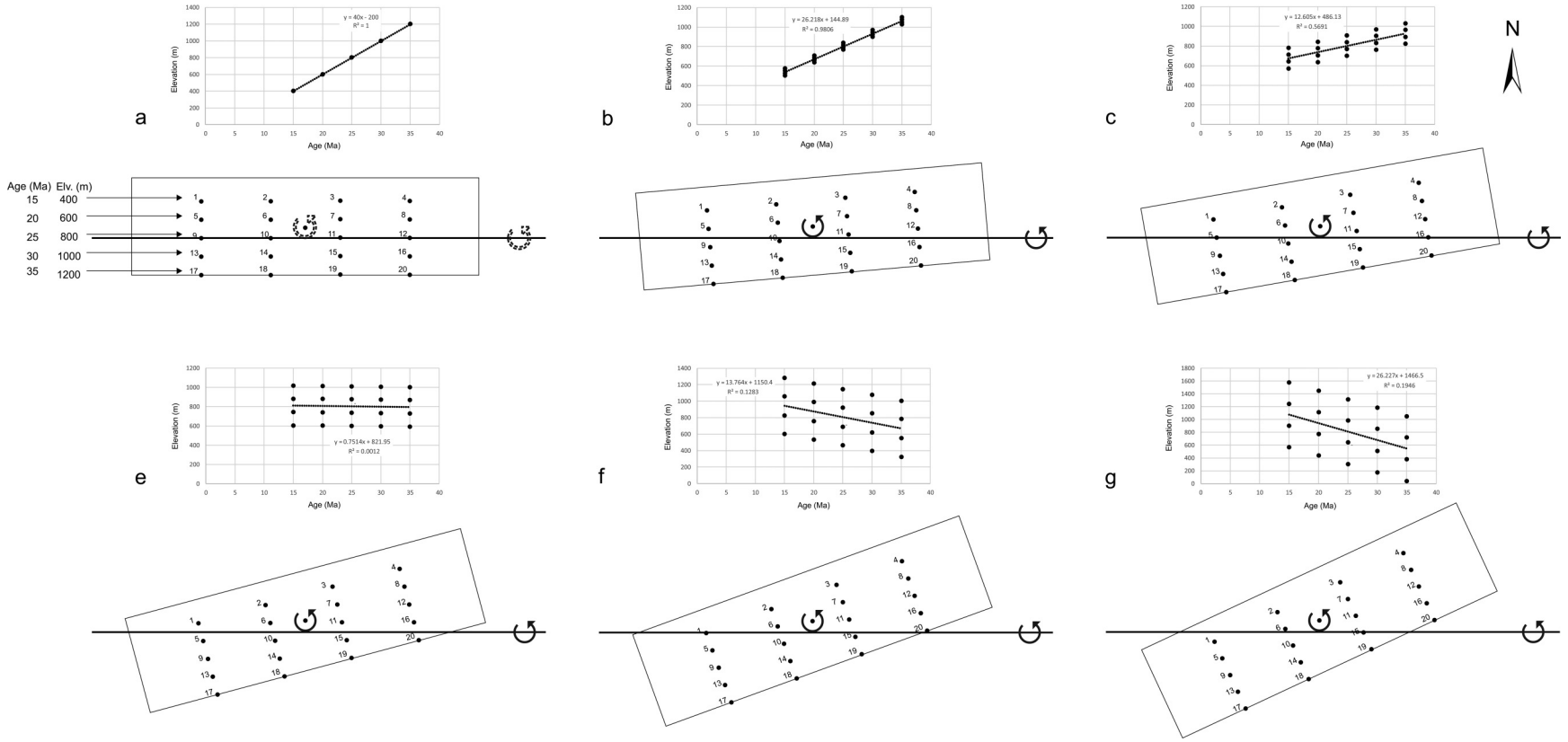

Fig. 7. Plausible fault scenarios that dissect former apatite (U–Th)/He age patterns. (*a*) Isochrone parallel (ISPA) axes dip-slip normal fault with planar fault plane, (*b*) ISPA dip-slip reverse fault with planar fault plane, (*c*) isochrone perpendicular (ISPE) axes dip-slip normal fault with planar fault plane, (*d*) ISPE dip-slip reverse fault with planar fault plane, (*e*) ISPA dip-slip normal fault with listric fault plane, (*f*) ISPA thrust fault with curvy planar fault plane, (*g*) ISPA strike-slip fault, (*h*) ISPE strike-slip fault. Orignal data are shown as white solid circles, whereas distorted data are illustrated as black solid circles. "F" indicates the flanks of the "Λ", and "t" indicates time. R, repetition; CO, clear offset; NVO, no vertical offset; ZD, zonal distribution.

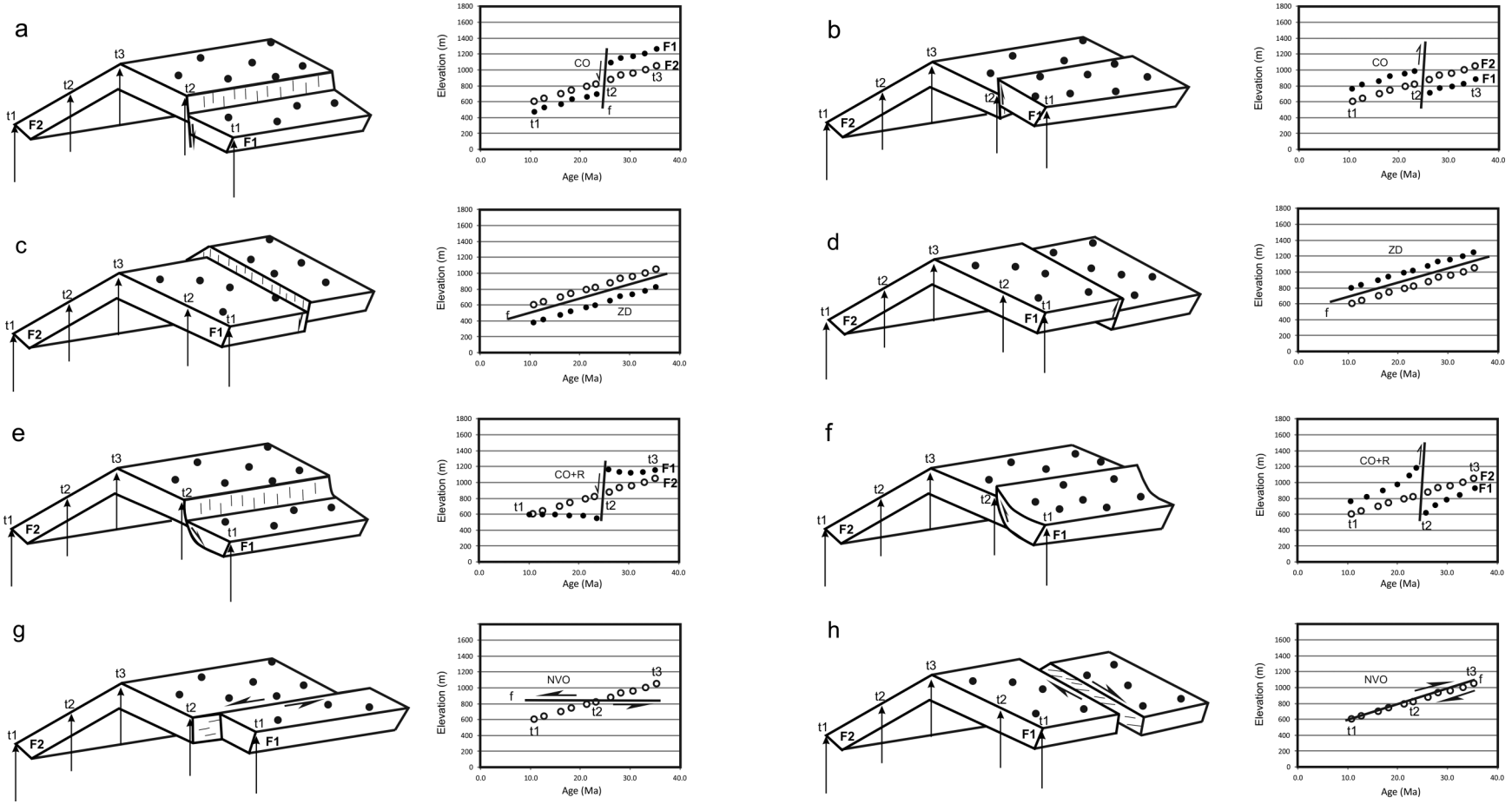

Fig. 8. Sorted and interpreted elevation vs. AHe age graphs. Note that there are four different trends in the Almacık Block. 1 has a low rate exhumation trend, and 2–4 have similarly high rate exhumation trends. There are two trends with almost identical exhumation rates in the southern part of the Middle Strand of the North Anatolian Fault Zone (NAFZ). See the text for details. R, rotation point.

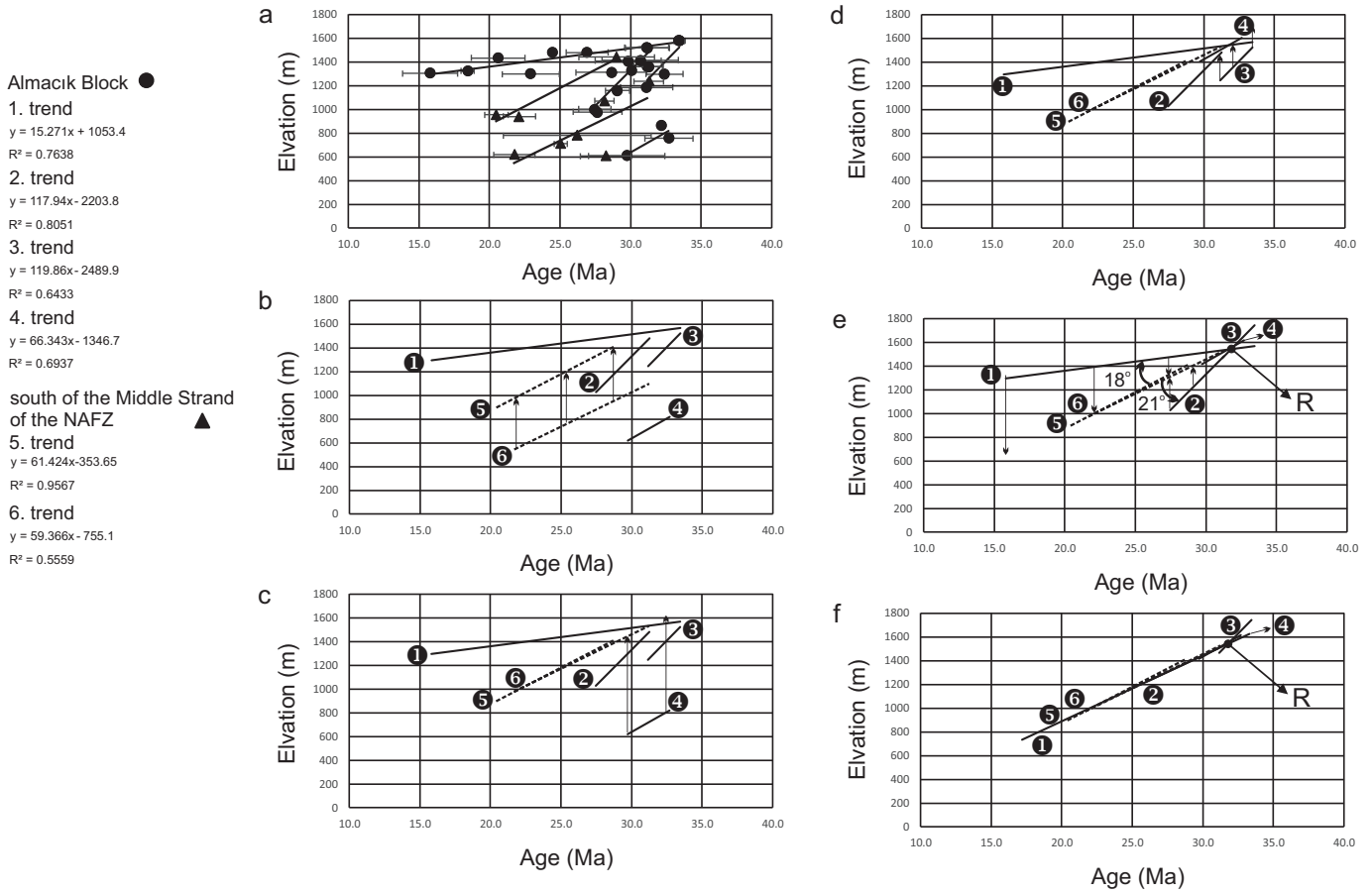

(Figs. 7*c* and 7*d*). However, along the southern part of the Middle Strand, there are splays of the NAFZ (Fig. 1). Such faults are mainly strike-slip faults, but they are parallel to the long axis of the deformation ellipsoid and perpendicular to the σ1, which indicates that they are oblique strike-slip faults with a reverse component. Some of the faults we infer in the region are not reported in the published fault maps (Emre et al. (2011), but the repetition in the age trends suggests the presence of these faults (see Figs. 1*b* and 3). Taking this into account, we individually calculated three different almost parallel exhumation rate groups: approximately 15 m/Myr (only one trend line #1 in Fig. 8), between 59 and 66 m/Myr (three trend lines #4, 5 and 6 in Fig. 8), and between 117 and 119 m/Myr (two trend lines #2 and 3 in Fig. 8).

The ages assigned to the PRZ and the NAFZ in the Almacık Block are less than those in the southern part of the Middle Strand (Fig. 2*a*). After data reduction, three exhumation trends can be distinguished. The first one has a more pronounced low exhumation rate (about 15 m/Myr, Fig. 8), the second one is represented by two more or less parallel high exhumation rates, and the third one has a moderate rate (Fig. 8). It is possible to interpret a high exhumation rate as a zonally distributed pattern. The constructed semi-parallel high exhumation rates give approximately117 and 119 m/Myr exhumation rates, respectively. Furthermore, the moderate rate of approximately 66 m/Myr (Fig. 8) is very close to the exhumation rate obtained from the southern part of the Middle Strand (Fig. 8). The lowest and the highest exhumation rates converge to a point making a wedge, which is highly typical for rotations where the axis is parallel to the isochrones (Figs. 5*a*–5*f*).

In each simulated case shown in Figs. 5*a*–5*f*, a wedge-shaped pattern of converging rates is observed. However, to confidently determine which simulation coincides roughly to the real case, an independent observation is needed from a region where deformation is relatively low or negligible. Without the knowledge about the initial exhumation rate, it is not possible to determine if any of the arms of the wedge are original or distorted. To determine the original arm of the wedge obtained in the Almacık Block (Figs. 8 and 9), we must analyze the southern part of the Middle Strand. In doing so, it may be possible to obtain the exhumation rate (Figs. 2 and 8) that can be used as the initial exhumation rate for the whole region (or at least the closest one).

Figure 8 shows recognized trend lines that belong to the whole region (Fig 8*a*), the general outline of them (Fig. 8*b*), and subsequent data reconstructions. Before proceeding further, we would like to explain our premise. The trend lines obtained from the southern part of the Middle Strand have similar slopes even though they are apart from each other (trends #5 and #6 in Fig. 8*b*). A similar case is also observed in the Almacık Block (trend #4 in Fig. 8*b*). Because the southern part of the Middle Strand is less deformed compared with the Almacık Block, we assume that approximately 60 m/Myr represents the initial (at least very close to initial) exhumation rate of the region. We further propose that the exhumation rates higher or lower than approximately 60 m/Myr are due to distortion of the original trends after rotation of the Almacık Block.

The trend lines obtained from the southern part of the Middle Strand are the same, but one is in the higher elevations (#5 in

Fig. 9. Trajectories of the exhumation trends given in Fig. 8. Each trend is numbered in both the graphs (top) and the map (bottom). The boundaries of each trace represent either a structural element or an axis of rotation. Later eliminations were performed due to overlaps of the traces of the trend lines in the map. The samples marked with a white open circle in the graphs were excluded from the final analyses. The white zones are the distribution of the partial retention zones (PRZs). The numbers in black circles are the trend numbers given in the graphs (and see also Fig. 8).

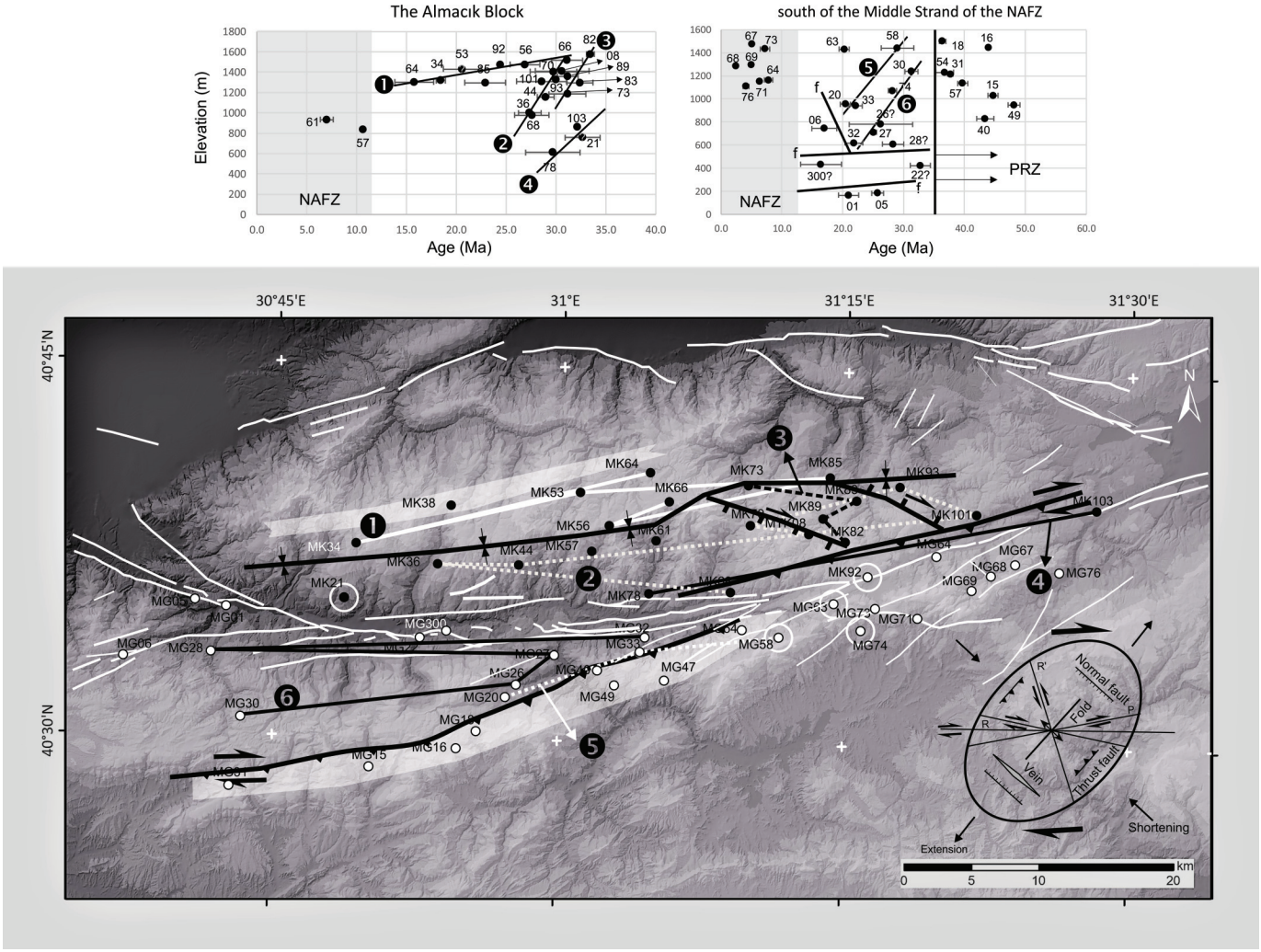

Fig. 8*b*) and the other is in the lower elevations (#6 in Fig. 8*b*). A similar trend line was also obtained from the Almacık Block (#4 in Fig. 8*b*). We think that approximately 60 m/Myr is most probably the real exhumation rate of the region and other rates are distorted because the southern part of the Middle Strand is less deformed compared with the Almacık Block. At least there are predictions about the deformation of the Almacık Block and one can expect more deformation in a thin and long block rather than a uniform southern part. Therefore, we assign the approximately 60 m/Myr rate as the original and less disturbed trend line for the region. If this is not the case, the method of reconstruction should be reconsidered.

The wedge shape of the trends from the Almacık Block (#1, #2, and #3 in Fig. 8*b*) surrounds the higher exhumation trend of the southern part of the Middle Strand (#5 in Fig. 8*b*). We interpreted these trends (#1, #2, #3, #4, and #6 in Fig. 8*b*) as being derived from trend #5 by various amounts of rotation and faulting, similar to the scenarios shown in Figs. 5 and 7. If this is the case, the trend line marked as #5 is the closest state to the original exhumation trend. If this inference is valid, all other trends should also be corrected according to the approximately 60 m/Myr rate (to #5 in Fig. 8*b*). During the correction processes it should be considered that the age data are solid, and the only variables are the elevations of the samples dated. Trend #6 is parallel to trend #5 but there is an approximately 453 m elevation difference between them (Fig. 8*b*). Thus, we must add this height to the samples constructing trend #6. Then, #6 will be corrected with respect to #5 (Fig. 8*c*). The only way to determine where to put a tectonic boundary or rotation axes to correct one apparent trend trajectory (#6) to the original one (#5) is to draw trend trajectories on the map (Fig. 9). We draw all trend trajectories (Fig. 8) on the topographic map of the region (Fig. 9). Every trajectory is constructed using relevant samples from the lowest and the youngest to the highest and the oldest (zig zag trajectories in Fig. 9). Considering trajectories #5 and 6, they are almost parallel to each other but there are some inconsistencies in some regions. However, it should be noted that the straight lines drawn between individual samples to construct trajectories could be curved lines. In the case of overlap, when samples fall within another trend, they are excluded from further calculations.

The only problem with trend #6 is that one of the samples that represents the upper end-member of the trend trajectory falls within the eastern part of the PRZ (in a different domain, see Fig. 9). Either the western or eastern part of the PRZ must be a

Fig. 10. Contoured AHe ages in the region. In the Almacık Block the contour lines (in black) are almost parallel to the long axis of the block, whereas in the south of the Middle Strand of the North Anatolian Fault Zone (NAFZ), they show a more complicated pattern (in dashed line). Ages in white with black backgrounds are uncertain ages (see Supplementary Table S2[2]).

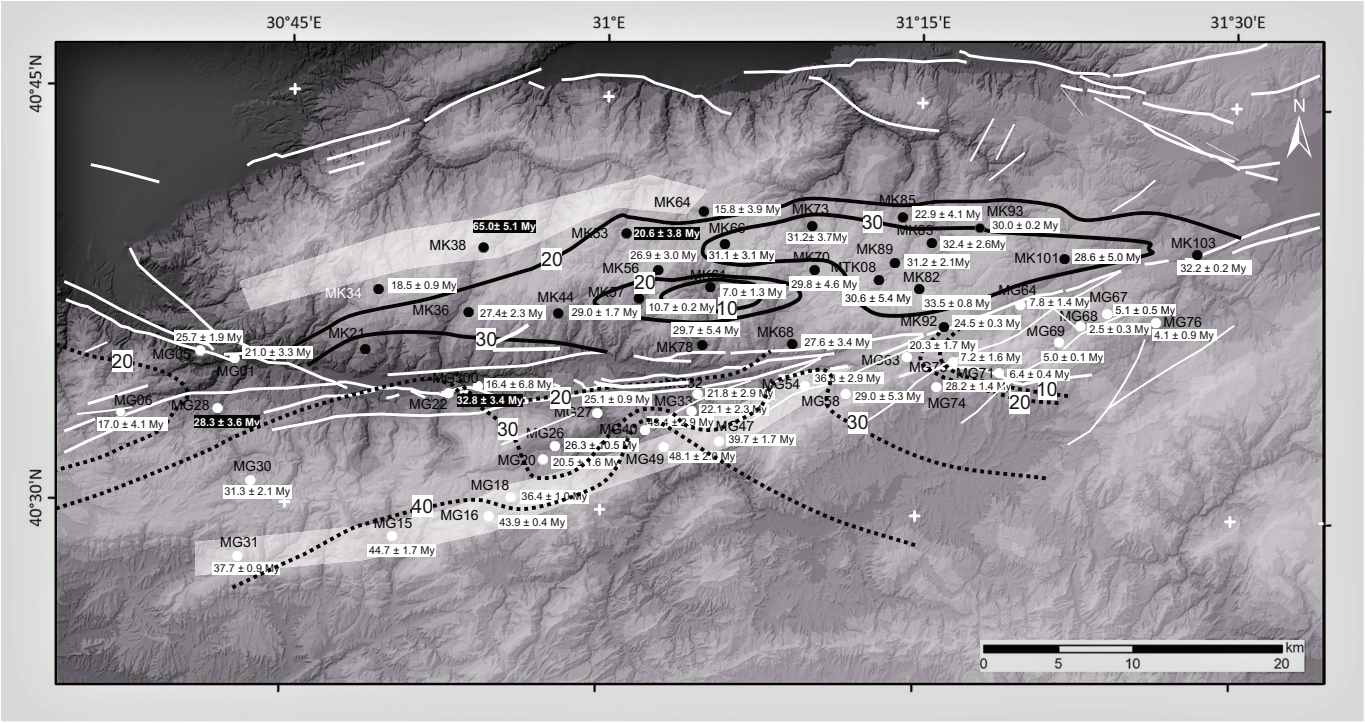

tectonic boundary because there are ages representing higher elevations on both sides of this belt. Thus, trend #6 may be artificial. Nonetheless, it still indicates that there must be a tectonic boundary between trends with different elevations (trends #5 and #6). The difference can be a reason for a possible fault boundary in the western part of the PRZ (a thrust in Fig. 9). If it is a fault, it should be a reverse fault because its alignment is perpendicular to the σ1 direction in a dextral strike-slip shear zone (Fig. 9).

A similar but much higher correction is also needed for trend #4 in the Almacık Block (Fig. 8*d*). The calculated elevation difference of the samples between trends #4 and #5 is about 845 m. Trajectory #4 is almost parallel to trajectories #5 and 6 and slightly oblique to the isochrones (Fig. 10). However, trend #4 is located in the Almacık Block, unlike trends #5 and 6. Therefore, the boundary for correction should be north of trajectory #4 instead of south where the middle part of the NAFZ is situated (Fig. 9). Similarly, because of its orientation in a given dextral strike-slip shear zone deformation ellipse, the possible tectonic boundary is assumed to be a reverse fault with a strike-slip component (Fig. 9).

The next correction is between trajectory lines #2 and #3 (Fig. 8), which are very close to each other and only a slight correction is needed. There is about 228 m elevation difference between them. For this correction, again trend trajectories should be drawn on the map to put a boundary or rotation axis (#2 and #3 in Fig. 9). However, trajectory #3 is located within trajectory #2. This situation cannot be resolved defining only one tectonic boundary between them, and at least two boundaries are necessary (Fig. 9). We defined two boundaries to constrain trend trajectory #3 on both sides (west and east sides). These boundaries are perpendicular to the isochrones (Fig. 10); hence, they match perfectly with the faults defined in Figs. 7*c* and 7*d*. Furthermore, their orientation corresponds to normal fault geometries in a given dextral strike-slip shear zone, and a dextral strike-slip component should also be expected (Fig. 9).

The last correction is to adjust trends #1 and 2 (Figs. 8*e* and 8*f*) to trend #5. Because trend #5 is the closest state of the original exhumation trend, the last correction would be similar to the situation shown in Figs. 8*e* and 8*f*. Around the rotation point R (Fig. 8*e*), the arms of the wedge must be closed by rotation. There are almost identical angles between trend #5 and other two trends (#1 and 2), which are 18° and 21°, respectively (Figs. 8*e* and 8*f*). The final state of the exhumation rate (fixed to trend #5, approximately 60 m/Myr) is now achieved for all trends (Fig. 8*f*).

Evolution of the Almacık Block in the NAFS

In Fig. 10, isochrones have been drawn separately for the Almacık Block and the southern part of the Middle Strand. The isochrones in the Almacık Block are almost parallel to the long axis of the block (east–west) as well as to the strike of the Middle Strand. The elevation difference between the actual and corrected heights of the AHe ages in the Almacık Block is shown in Fig. 11 where the "0" contour represents the rotation axis along which there is no change in the elevations. Figure 12 shows the summary tectonic map for the region with tectonic features obtained from AHe ages. Although samples were uplifted on the northern side of the rotation axis, they subsided on the southern side (see also Fig. 13). For example, according to the last correction, sample MK 64 (the northernmost sample) was uplifted about 684 m during the NAFZ activity. When we extend our analyses of deformation to the whole northern part of the Almacık Block, the northernmost rim of the block should be uplifted to a height of 2800 m. Similarly, the calculated uplift amount from the higher rate correction (trends #2 and #3 in Fig. 8) is about 365 m for sample MK 68 (the southernmost sample). Note that trend #3 is corrected twice. When we extend this bending to the southernmost part of the block until the middle strand of the NAFZ, amount of the uplift is about 431 m.

Unfortunately, few studies have been performed on the vertical exhumation of the Almacık block. One of the recent studies on

Fig. 11. Contour map of the elevation differences between the actual and corrected heights of the samples (white numbers with black backgrounds) in the Almacık Block (in meters). White numbers indicate contour intervals. The 0 m contour line represents the rotation axis on which there is no elevation change. The region with positive numbers shows uplifted areas whereas the region with negative numbers shows subsided areas. PRZ, partial retention zone.

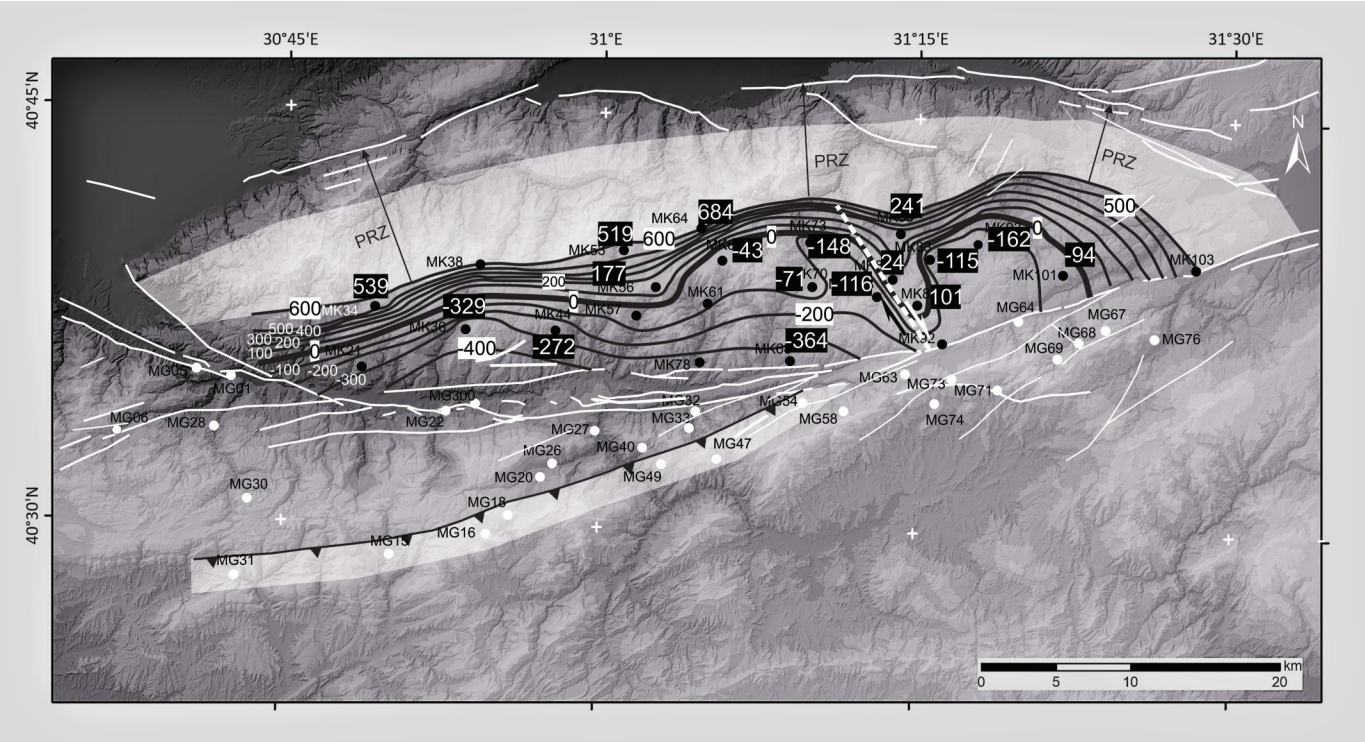

Fig. 12. The summary structural map of the Almacık Block and its southern part. Thick lines are our structural estimations derived from analyses of the AHe ages. PRZ, partial retention zone.

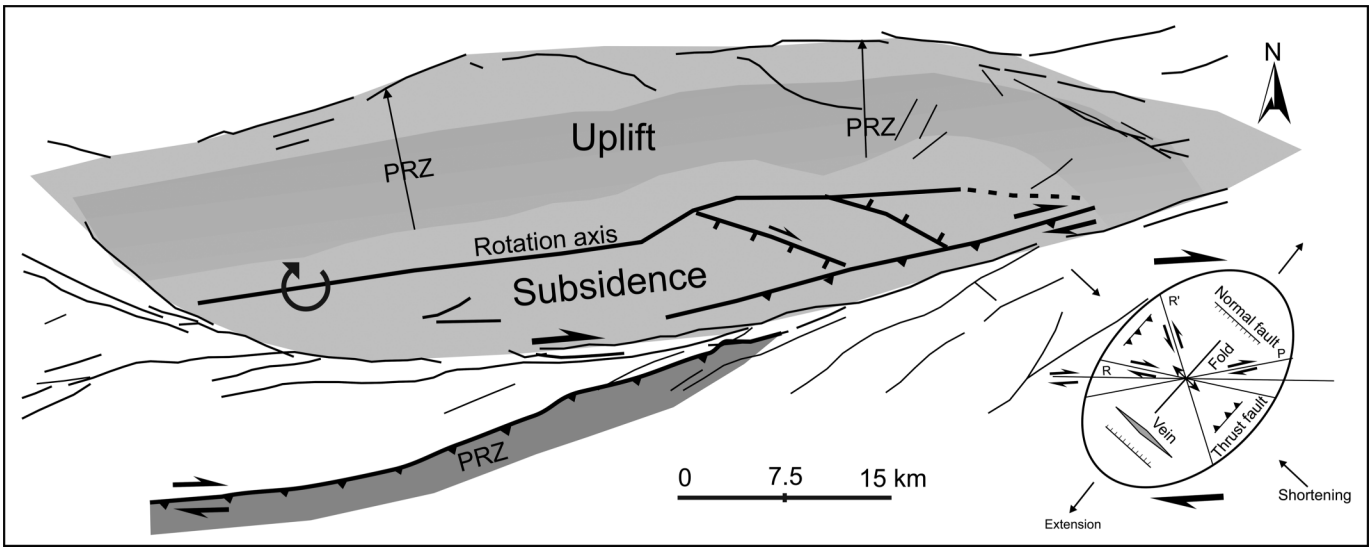

the tectonics of the Almacık Block is by Yıldırım and Tüysüz (2017). Using morphological indicators, they claimed that the Almacık Block has 20° ± 2° clockwise rotation about the vertical axis and that the calculated surface uplift is 1130 ± 130 m. This value includes both exhumation and the accompanied erosion. Our estimated value represents only the amount of exhumation without erosion.

The northern boundary of the Almacık Block is a north-dipping dextral strike-slip fault with normal component, which was ruptured during the 1999 earthquakes (Barka et al. 2002; Akyüz et al. 2002; Çakır et al. 2003*a*, 2003*b*; Bulut et al. 2007). During the Izmit earthquake, the western part of the northern edge of the Almacık Block was ruptured in the Karadere region (Fig. 1). The trend of the rupture is approximately southwest–northeast-directed and defines the northwest termination of the Düzce Basin. During the Düzce earthquake, the rest of the boundary of the Almacık Block broke again three months after the İzmit earthquake (Akyüz et al. 2002). Akyüz et al. (2002) reported offset measurements observed right after the Düzce earthquake. Numerous vertical separations were reported in addition to the dextral offsets, which indicates

Fig. 13. East-looking model of the Almacık Block. Note that during the clockwise rotation the northern part of the block has uplifted, whereas the southern part has subsided. NAFZ, North Anatolian Fault Zone; PRZ, partial retention zone; RP, rotation pole. [Color online.]

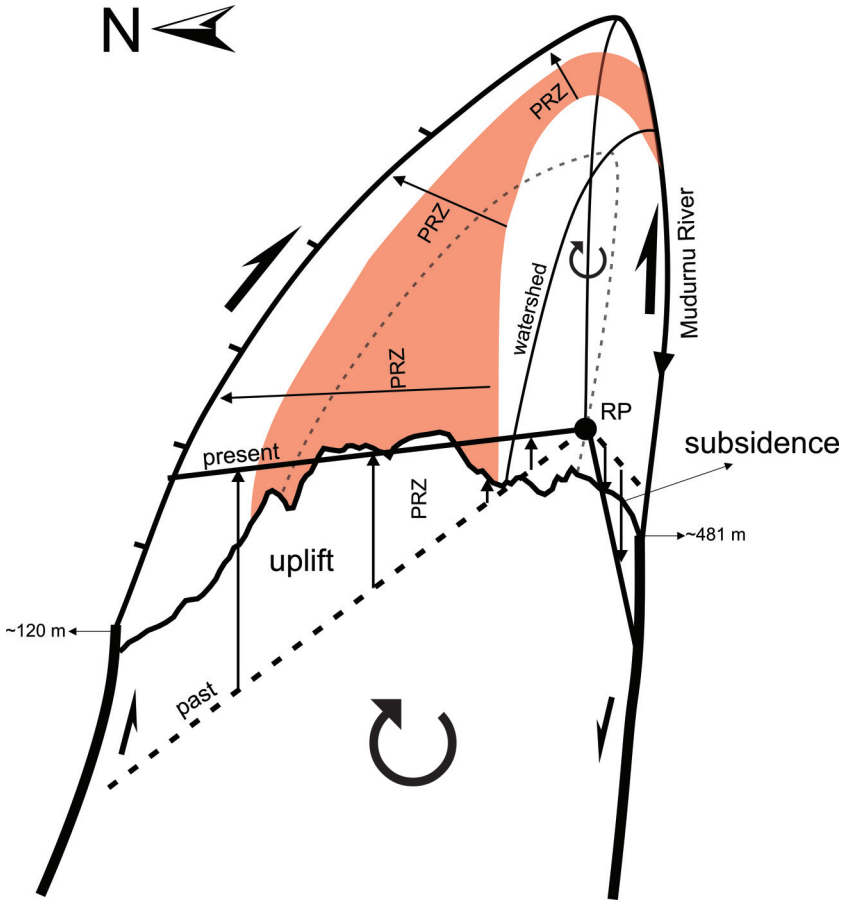

that the northern part of the Almacık Block was uplifted. Up to 3.5 meters of vertical displacement along the surface rupture were reported, but in general they were about 30 cm (Akyüz et al. 2002). Assuming the observed maximum vertical separation of 3.5 m as a characteristic fault slip, creating an uplift of about 2800 m on the northernmost edge of the block takes around 200 000 years assuming a 250 year earthquake occurrence (Barka 1996; Parsons 2004; Şengör et al. 2005; Bohnhoff et al. 2013; Ergintav et al. 2014), whereas when we account for an average vertical separation of 0.03 m, such an amount of uplift takes about 2.3 Ma.

Even if we assign the ages younger than 12 Ma to the activity of the NAFZ, the concentration of the young ages was found to be between 7.8 and 2.5 Ma (supplementary data Table S2[2]). It is possible to interpret older ages as the age of the shear zone of the NAFZ, but younger ones at around 2.5 Ma are most likely representing the age the NAF. This inference can also be correlated with the formation of the wide pull-apart Adapazari Basin in the west of the Almacık Block where the earliest deposition is dated back to the latest Villanyian (latest Pliocene) and the Biharian (early Pleistocene) (~3 Ma, Ünay et al. 2001). If the region began to uplift at 7.8 Ma, the uplift rate would be calculated as about 359 m/Myr. Such a trend is seven times more than the rate (about 60 m/Myr) obtained for regional exhumation in the region. As a result, if we take the age of the NAF to be 2.5 Ma in the region, it is still enough to generate the calculated amount of uplift.

The southern boundary of the Almacık Block also was ruptured by earthquakes during the last century (1944 Bolu-Gerede, 1957 Abant, and 1967 Mudurnu Valley earthquakes) (Barka 1992; Barka et al. 2002; Akyüz et al. 2002; Kondo et al. 2005, 2010; Duman et al. 2005; Pucci et al. 2007; Seyitoğlu et al. 2015). However, the reported offset measurements from the 1967 Mudurnu Valley earthquake rupture do not show any preferred uplift side along its course (Ambraseys and Zatopek 1969; Barka 1996).

The younger ages between 7.8 and 2.5 Ma are obtained from the southeastern part of the study area (Fig. 3). Such ages are clustered in the region where the Jurassic Mudurnu Formation is exposed (supplementary Fig. S1[2]). This region is represented by dense fault branches related to the Middle Strand of the NAFZ. The proposed reset is most likely related to the hot fluid activity that occurred during the active period of the NAFZ. Today, in the western part of this region, along the Middle Strand of the NAFZ, there are two places famous for their hot springs, namely Kuzuluk and Taşkesti. The southeastern part of the studied area may be a former and similar hot fluid discharge region.

Another outcome of this study is the inference of potentially active normal and thrust faults that were not reported previously in the region (see the geological map (Supplementary Fig. S1[2]) by Gedik and Aksay 2002). The reason for the absence of these faults on the published geological maps is likely that they had not been discovered yet, or that the PRZ we defined is just a thin Eocene cover in this narrow zone that was a paleo-ridge that formed before the Eocene deposition. Thus, deposition would be thin over the ridge and did not lead to complete reset in the samples. However, there is no information about the second possibility; in any case, such a linear ridge was most probably bounded by a tectonic line(s).

Similarly, the normal faults estimated by AHe ages (Fig. 12) are not present in the geological maps published by Gedik and Aksay 2002). These faults are located mainly in the Upper Cretaceous units and could easily be missed.

As stated before, all the ages older than 36 Ma (the youngest age of the Eocene cover, Gülmez et al. 2013) are regarded as the PRZ. In the south they are aligned along a zone, but in the north they are represented by only one age (around 65 Ma, MK 38). Its continuation as a zone to the east and the west is not clear. Furthermore, contouring AHe ages and the elevation differences (Figs. 10 and 12) reveals how isochrones are distributed in the region (Fig. 11). Therefore, it allows us to extend the zone of the PRZ all along the Almacık Block (Figs. 11 and 12). To check this estimation, if the position of the PRZ is in the right place, one can control the distribution of the AHe ages that must be getting older when moving away from the PRZ.

Early studies of the horizontal rotation revealed different results. Şengör et al. (1985) used the position of the IPSZ to determine the amount of rotation in the region and obtained a result of 110° clockwise rotation. This inference is sensible because, except for the Almacık Block, the orientation of the IPSZ is approximately east–west (see Fig. 1). However, in the Almacık Block, its orientation is approximately northeast–southwest separating the Istanbul Zone in the southeast from the Sakarya Zone in the northwest, which is in opposite directions in other parts of the IPSZ. 212° and 28° clockwise rotations were proposed according to the paleomagnetic studies performed on Eocene volcanic rocks (Sarıbudak et al. 1990; İşseven et al. 2009). The rotation amounts outlined so far contradict each other because they all include post-Eocene rotation. The 212° clockwise rotation looks unlikely because the Istanbul and the Sakarya Zones remain in the wrong geographical sides of the suture when the rotation is restored. The 28° clockwise rotation also seems unlikely because the IPSZ is aligned roughly north–south when the rotation is restored, but in general, its position is approximately east–west. A recent study reported approximately 20° clockwise rotation calculated from the morphological features (Yıldırım and Tüysüz 2017) that formed during and (or) after the development of the Pliocene paleotopography of the region (see Yıldırım and Tüysüz 2017 for detailed discussion and additional references). Furthermore, 110° and 20° clockwise rotations can be both valid because they include rotations for different tine intervals. Recent studies have shown that before the initiation of the NAFZ in the region an early fault system was active (Zattin et al. 2010; Akbayram et al. 2016*b*). Zattin et al. (2010) proposed that there was a fault system (mainly dip-slip) formed before the inception of the NAFZ in the region. Furthermore, Akbayram et al. (2016*b*) claimed that during and after the closure of the IPSZ a dextral strike-slip fault system predated the NAFZ. If so, the 110° clockwise rotation proposed by Şengör et al. (1985) represents the long-term rotation (Ypresian to recent) whereas the 20° clockwise rotation reported by Yıldırım and Tüysüz (2017) represents the short-term rotation (i.e., only the effect of the NAFZ). The horizontal rotation around the vertical axis could not be confirmed by this study because we mainly have data about the rotation along the horizontal and sub-horizontal axes. In other words, we can detect movements mainly in the vertical sense.

Conclusions

Before the inception of the NAFZ in the region, the northwestern part of the Anatolian block started to exhume at about 34 Ma (Rupelian) and lasted until about 16 Ma (Langhian). Even if different rates have been achieved, the most probable average exhumation rate was about 60 m/Myr.

Different structural models distorting the AHe age–elevation trends have been tested and illustrated to understand the behavior of the NAFZ on the Almacık Block.

Reconstructions made on the distorted AHe age trends revealed the following results.

- Distorted exhumation trends hint at the presence of previously unreported northwest–southeast-trending normal and northeast–southwest-trending reverse faults both in the Almacık Block and southern part the Middle Strand of the NAFZ.
- The Almacık Block is rotated about a roughly east–west-trending horizontal axis. While the northern part of the block was uplifting, the southern part was subsiding.
- The northernmost edge of the block has been uplifted roughly 2800 m probably during the last 2.5 Ma, but the southernmost part of the block has subsided around 430 m.
- The activity of the NAFZ in the region most likely started later than 8 Ma, but the most intensive deformation took place around 2.5 Ma. Here, we interpret these two dates as the activity of the early shear zone of the NAF in the region and the initiation of the NAF itself, respectively.

Acknowledgements

This study was supported by TÜBITAK (The Scientific and Technical Research Council of Turkey, Project no: CAYDAG 109Y257) and the Istanbul Technical University (BAP Project No. MGA-2018-41082). We would like to thank W. Cawazza and two anonymous reviewers for very careful and constructive reviews, and A. Polat for his review and editorial handling.

References

Abdüsselamoğlu, M.S. 1959. Almacıkdağı ile Mudurnu ve Göynük Civarının Jeolojisi [Geology of Almacıkdağı, Mudurnu and Göynük Region]. Istanbul Üniversitesi, Fen Fakültesi Monografileri, **14**: 1–94.

Akbayram, K., Okay, A.I., and Satır, M. 2013. Early Cretaceous closure of the Intra-Pontide Ocean in western Pontides (northwestern Turkey). Journal of Geodynamics, **65**: 38–55. doi:10.1016/j.jog.2012.05.003.

Akbayram, K., Sorlien, C.C., and Okay, A.I. 2016*a*. Evidence for a minimum 52±1 km of total offset along the northern branch of the North Anatolian Fault in northwest Turkey. Tectonophysics, **668–669**: 35–41. doi:10.1016/j.tecto.2015.11.026.

Akbayram, K., Şengör, A.M.C., and Özcan, E. 2016*b*. The evolution of the Intra-Pontide suture: Implications of the discovery of late Cretaceous–early Tertiary mélanges. The Geological Society of America Special Paper 525, In Honor of Manuel Berberian's Forty-Five Years of Research Contributions. doi:10.1130/2016.2525(18).

Akyüz, H.S., Hartleb, R., Barka, A., Altunel, E., Sunal, G., Meyer, B., and Armijo, R. 2002. Surface rupture and slip distribution of the 12 November 1999 Düzce earthquake (M 7.1), North Anatolian fault, Bolu, Turkey. Bulletin of the Seismological Society of America, **92**(1): 61–66. doi:10.1785/0120000840.

Altiner, D., Koçyiğit, A., Farinacci, A., Nicosia, U., and Conti, M.A. 1991. Jurassic–Lower Cretaceous stratigraphy and paleogeographic evolution of the southern part of North-Western Anatolia (Turkey). Geologica Romana, **27**: 13–81.

Ambraseys, N.N., and Zatopek, A. 1969. The Mudurnu valley, West Anatolia, Turkey, earthquake of 22 July 1967. Bulletin of the Seismological Society of America, **59**: 521–589.

Ballato, P., Parra, M., Schildgen, T.F., Dunkl, I., Yıldırım, C., Özsayın, E., et al. 2018. Multiple exhumation phases in the Central Pontides (N Turkey): new temporal constraints on major geodynamic changes associated with the closure of the Neo-Tethys Ocean. Tectonics, **37**(6): 1831–1857.

Barka, A.A. 1992. The North Anatolian Fault Zone. Annales Tectonicae, **6**: 164–195.

Barka, A.A. 1996. Slip distribution along the North Anatolian Fault associated with large earthquakes of period 1939 to 1967. Bulletin of the Seismological Society of America, **86**: 1238–1254.

Barka, A.A., and Kadinsky-Cade, K. 1988. Strike-slip fault geometry in Turkey and its influence on earthquake activity. Tectonics, **7**: 663–684. doi:10.1029/TC007i003p00663.

Barka, A., Akyüz, S.H., Altunel, E., Sunal, G., Çakir, Z., Dikbaş, A., et al. 2002. The surface rupture and slip distribution of the 17 August 1999 İzmit earthquake M=7.4, North Anatolian Fault. Bulletin Seismological Society of America, **92**: 43–60. doi:10.1785/0120000841.

Bohnhoff, M., Bulut, F., Dresen, G., Malin, P., Eken, T., and Aktar, M. 2013. An earthquake gap south of Istanbul. *In* Nature communications. 4. 1999. https://doi.org/10.1038/ncomms2999.

Bozkurt, E., Winchester, J.A., Satir, M., Crowley, Q.G., and Ottley, C.J. 2013. The Almacık mafic-ultramafic complex: exhumed Sakarya subcrustal mantle adjacent to the Istanbul Zone, NW Turkey. Geological Magazine, **150**(2): 254–282. doi:10.1017/S0016756812000556.

Bulut, F., Bohnhoff, M., Aktar, M., and Dresen, G. 2007. Characterization of aftershock-fault plane orientations of 1999 İzmit (Turkey) earthquake using high-resolution aftershock locations. Geophysical Research Letters, **34**: L20306. doi:10.1029/2007GL031154.

Çakır, Z., Barka, A., and Evren, E. 2003*a*. Coulomb stress interactions and the 1999 Marmara Earthquake sequence. Turkish Journal of Earth Sciences, **12**: 91–103.

Çakır, Z., Barka, A., de Chabalier, J.-B., Armijo, R., and Meyer, B. 2003*b*. Kinematics of the November 12, 1999 (Mw=7.2) Düzce earthquake deduced from SAR interferometry, Turkish Journal of Earth Sciences, **12**: 105-118.

Cavazza, W., Cattò, S., Zattin, M., Okay, A.I., and Reiners, P. 2018. Thermochronology of the Miocene Arabia-Eurasia collision zone of southeastern Turkey. Geosphere; **14**(5): 2277–2293. doi:10.1130/GES01637.1.

Çelik, Ö.F., Gürer, Ö.F., Aldanmaz, E., Spell, T., and Öz, İ. 2009. Armutlu Yarımadası ve Almacıkdağ Amfibolitik Kayaçları İçin İzotopik ve Jeokimyasal Sınırlamalar. 62. Türkiye Jeoloji Kurultayı, MTA Ankara, pp. 466–467.

Chen, F., Siebel, W., Satir, M., Terzioğlu, N., and Saka, K. 2002. Geochronology of the Karadere basement (NW Turkey) and implications for the geological evolution of the İstanbul Zone. International Journal Earth Sciences, **91**: 469–481. doi:10.1007/s00531-001-0239-6.

Duman, T., Emre, Ö., Doğan, A., and Özalp, S. 2005. Step-over and bend structures along the 1999 Düzce earthquake surface rupture, North Anatolian Fault, Turkey. Bulletin of the Seismological Society of America, **95**(4): 1250–1262. doi:10.1785/0120040082.

Ehlers, T.A., and Farley, K.A. 2003. Apatite (U–Th)/He thermochronometry: methods and applications to problems in tectonic and surface processes. Earth and Planetary Science Letters, **206**(1–2): 1–14. doi:10.1016/S0012-821X(02)01069-5.

Emre, Ö., Duman, T.Y., and Özalp, S. 2011. 1:250,000 scale active fault map series of Turkey, Adapazarı (NK36-13) Quandrangle. Serial Number: 14, General Directiorate of Mineral Research and Exploration, Ankara-Turkey.

Ergintav, S., Reilinger, R.E., Çakmak, R., Floyd, M., Çakır, Z., Dogan, U., et al. 2014. Istanbul's earthquake hot spots: Geodetic constraints on strain accumulation along faults in the Marmara Seismic Gap. Geophysical Research Letters, **41**: 5783–5788. doi:10.1002/2014GL060985.

Farley, K.A. 2002. (U-Th)/He dating; techniques, calibrations, and applications. *In* Noble gases in geochemistry and cosmochemistry. *Edited by* D. Porcelli, C.J. Ballentine, and R. Wieler. Reviews in Mineralogy and Geochemistry, 47: 819–843. [Mineralogical Society of America.]

Farley, K.A., Wolf, R., and Silver, L. 1996. The effects of long alpha-stopping distances on (U-Th)/He ages. Geochimica et Cosmochimica Acta, **60**(21): 4223–4229. doi:10.1016/S0016-7037(96)00193-7.

Fitzgerald, P.G., and Gleadow, A.J.W. 1990. New approaches in fission track geochronology as a tectonic tool: examples from the Transantarctic Mountains. Nuclear Tracks, **17**: 351–357. doi:10.1016/1359-0189(90)90057-5.

Fitzgerald, P.G., Baldwin, S.L., Webb, L.E., and O'Sullivan, P.B. 2006. Interpretation of (U–Th)/He single grain ages from slowly cooled crustal terranes: A case study from the Transantarctic Mountains of southern Victoria Land. Chemical Geology, **225**(1–2): 91–120. doi:10.1016/j.chemgeo.2005.09.001.

Gedik, İ., and Aksay, A. 2002. 1: 100000 ölçekli Türkiye Jeoloji Haritaları Adapazarı G25 paftası. No. 32. MTA Genel Müdürlüğü, Ankara.

Genç, Ş.C., and Tüysüz, O. 2010. Tectonic setting of the Jurassic bimodal magmatism in the Sakarya Zone (Central and Western Pontides), northern Turkey: a geochemical and isotopic approach. Lithos, **118**: 95–111. doi:10.1016/j.lithos.2010.03.017.

Green, P.F., and Duddy, I.R. 2006. Interpretation of apatite (U–Th)/He ages and fission track ages from cratons. Earth and Planetary Science Letters, **244**(3–4): 541–547. doi:10.1016/j.epsl.2006.02.024.

Gülmez, F., Genç, S.C., Keskin, M., and Tüysüz, O. 2013. A post-collision slab-breakoff model for the origin of the Middle Eocene magmatic rocks of the Armutlu–Almacik belt, NW Turkey and its regional implications. *In* Geological development of Anatolia and the Easternmost Mediterranean Region. *Edited by* A.H.F. Robertson, O. Parlak, and U.C. Ünlügenç. Geological Society Special Publication, **372**: 107–139.

Hisarlı, Z.M., Cengiz Çinku, M., and Orbay, N. 2011. Paleomagnetic evidence of complex tectonic rotation pattern in the NW Anatolian Region: Implications for the Tectonic History since the Middle Eocene. Tectonophysics, **505**: 86–99. doi:10.1016/j.tecto.2011.04.005.

İşseven, T., Demir, T., Genç, Ş.C., and Gülmez, F. 2009. How has strike slip motion on the North Anatolian Fault rotated the Almacık block? 62. *In* Geological Congress of Turkey, MTA Ankara, pp. 936–937.

Keskin, M., Genç, Ş.C., and Tüysüz, O. 2008. Petrology and geochemistry of post-collisional Middle Eocene volcanic units in North- Central Turkey: evidence for magma generation by slab breakoff following the closure of the Northern Neotethys Ocean. Lithos, **104**: 267–305. doi:10.1016/j.lithos.2007.12.011.

Ketin, İ. 1948. Über die tektonisch-mechanischen Folgerungen aus den grossen anatolischen Erdbeben des letzten Dezenniums. Geol. Rund. **36**: 77–83.

Ketin, İ. 1969. Kuzey Amadolu Fayı hakkında. Maden Tatkik Arama Ens. Derg. **72**: 1–27.

Kondo, H., Awata, Y., Emre, Ö., Doğan, A., Özalp, S., Tokay, F., et al. 2005. Slip distribution, fault geometry, and fault segmentation of the 1944 Bolu-Gerede earthquake rupture, North Anatolian fault, Turkey. Bulletin of the Seismological Society of America, **95**(4): 1234–1249. doi:10.1785/0120040194.

Kondo, H., Özaksoy, V., and Yıldırım, C. 2010. Slip history of the 1944 Bolu-Gerede earthquake rupture along the North Anatolian fault system: Implications for recurrence behavior of multisegment earthquakes. Journal of Geophysical Research: Solid Earth, **115**: B0431. doi:10.1029/2009JB006413.

Lom, N., Ülgen, S.C., Sakınç, M., and Şengör, A.M.C. 2016. Geology and stratigraphy of Istanbul region. *In* Late Miocene mammal locality of Küçükçekmece, European Turkey *Edited by* Ş. Şen. Geodiversitas, **38**(2): 175–195. doi:10.5252/g2016n2a3.

NASA JPL. 2013. NASA Shuttle Radar Topography Mission Global 3 arc second. Distributed by NASA EOSDIS Land Processes. doi:10.5067/MEaSUREs/SRTM/SRTMGL3.003.

Okay, A.I., and Göncüoğlu, C.M. 2004. The Karakaya complex: A review of data and concepts. Turkish Journal of Earth Sciences, **13**: 77–95.

Parsons, T. 2004. Recalculated probability of M ≥ 7 earthquakes beneath the Sea of Marmara, Turkey. Journal of Geophysical Research: Solid Earth, **109**: B05304. doi:10.1029/2003JB002667.

Pucci, S., Pantosti, D., Barchi, M.R., and Palyvos, N. 2007. A complex seismogenic shear zone: the Düzce segment of North Anatolian Fault (Turkey). Earth and Planetary Science Letters, **262**(1–2): 185–203. doi:10.1016/j.epsl.2007.07.038.

Reiners, P.W., Zhou, Z., Ehlers, T.A., Xu, C., Brandon, M.T., Donelick, R.A., and Nicolescu, S. 2003. Post-orogenic evolution of the Dabie Shan, eastern China, from (U-Th)/He and fission-track thermochronology. American Journal of Science, **303**: 489–518. doi:10.2475/ajs.303.6.489.

Reiners, P.W., Carlson, R.W., Renne, P.R., Cooper, K.M., Granger, D.E., McLean, N.M., and Schoene, B. 2017. Geochronology and thermochronology. John Wiley & Sons Ltd.

Sarıbudak, M., Sanver, M., Şengör, A.M.C., and Görür, N. 1990. Palaeomagnetic evidence for substantial rotation of the Almacık Flake within the North Anatolian Fault Zone, northwest Turkey. Geophysical Journal International, **102**: 563–568. doi:10.1111/j.1365-246X.1990.tb04582.x.

Şengör, A.M.C. 1979. The North Anatolian Transform Fault: its age, offset and tectonic significance. J. Geol. Soc. (Lond.), **136**: 269–82. doi:10.1144/gsjgs.136.3.0269.

Şengör, A.M.C., and Yılmaz, Y. 1981. Tethyan evolution of Turkey: A plate tectonic approach. Tectonophysics, **75**: 181–241. doi:10.1016/0040-1951(81)90275-4.

Şengör, A.M.C., and Zabcı, C. 2019. The North Anatolian Fault and the North Anatolian Shear Zone. *In* Landscapes and landforms of Turkey. *Edited by* C. Kuzucuoğlu, A. Çiner, and N. Kazancı. Springer International Publishing, Cham. pp. 481–494. doi:10.1007/978-3-030-03515-0_27.

Şengör, A.M.C., Görür, N., and Şaroğlu, F. 1985. Strike-slip faulting and related basin formation in zones of tectonic escape: Turkey as a case study. *In* Strike-slip Deformation, Basin Formation, and Sedimentation. *Edited by* K.T. Biddle and N. Christie-Blick. The Society of Economic Paleontologists and Mineralogists. 37 (in honor of J.C. Crowell), pp. 227–264.

Şengör, A.M.C., Tüysüz, O., İmren, C., Sakınç, M., Eyidoğan, H., Görür, N., Le Pichon, X., and Rangin, C. 2005. The North Anatolian Fault: a new look. Annual Review of Earth and Planetary Sciences, **33**(1): 37–112. doi:10.1146/annurev.earth.32.101802.120415.

Seyitoğlu, G., Ecevitoğlu, B., Kaypak, B., Esat, K., Çağlayan, A., Gündoğdu, O., Güney, Y., Işık, V., Pekkan, E., Tün, M., and Avdan, U. 2015. A missing-link in the tectonic configuration of the Almacık Block along the North Anatolian Fault Zone (NW Turkey): active faulting in the Bolu plain based on seismic reflection studies. Geophysical Journal International, **201**(3): 1814–1833.

Stockli, D. 2005. Application of low-temperature thermochronometry to extensional tectonic settings: techniques, interpretations, and applications. Reviews in Mineralogy & Geochemistry, **58**: 411–448. doi:10.2138/rmg.2005.58.16.

Stübner, K., Grujic, D., Dunkl, I., Thiede, R., and Eugster, P. 2018. Pliocene episodic exhumation and the significance of the Munsiari thrust in the northwestern Himalaya. Earth and Planetary Science Letters, **481**: 273–283. doi:10.1016/j.epsl.2017.10.036.

Sunal, G., and Erturaç, M.K. 2012. Estimation of the pre-North Anatolian Fault Zone pseudo-paleo-topography: A key to determining the cumulative offset of major post-collisional strike slip faults. Geomorphology, **159–160**: 125–141. doi:10.1016/j.geomorph.2012.03.013.

Ünay, E., Emre, Ö., Erkal, T., and Keçer, M. 2001. The rodent fauna from the Adapazari pull-apart basin (NW Anatolia): Its bearings on the age of the North Anatolia fault. Geodinamica Acta, **14**: 169–175. doi:10.1016/S0985-3111(00)01063-9.

Yıldırım, C., and Tüysüz, O. 2017. Estimation of the long-term slip, surface uplift and block rotation along the northern strand of the North Anatolian Fault Zone: Inferences from geomorphology of the Almacık Block. Geomorphology, **297**: 55–68. doi:10.1016/j.geomorph.2017.08.038.

Zattin, M., Okay, A.I., and Cavazza, W. 2005. Fission-track evidence for late Oligocene and mid-Miocene activity along the North Anatolian Fault in southwestern Thrace. Terra Nova, **17**: 95–101. doi:10.1111/j.1365-3121.2004.00583.x.

Zattin, M., Cavazza, W., Okay, A.I., Federici, I., Fellin, M.G., Pignalosa, A., and Reiners, P. 2010. A precursor of the North Anatolian Fault in the Marmara Sea region. Journal of Asian Earth Sciences, **39**: 97–108. doi:10.1016/j.jseaes.2010.02.014.